Offshore forecasting of Hawaiian tsunamis generated in Alaskan-Aleutian Subduction Zone

Vasily V. Titov, Harold O. Mofjeld, Frank I. González, and
Jean C. Newman

January 1999

Contents

Offshore forecasting of Hawaiian tsunamis generated in Alaskan-Aleutian Subduction Zone

Vasily V. Titov, Harold O. Mofjeld, Frank I. González, and
Jean C. Newman

Abstract. This report describes an R&D activity conducted during FY 1998 to develop tsunami forecasting tools for the Pacific Disaster Center (PDC). The activity included analytical and numerical sensitivity studies of tsunami wave characteristics offshore of Hawaii, for ranges of earthquake source parameters in the Alaska-Aleutian Subduction Zone (AASZ); this region is a major source of destructive tsunamis that strike Hawaii. A set of tsunami numerical simulation scenarios was designed to be the basis for the sensitivity analysis, using the 1996 Andreanov Island earthquake/tsunami as a reference. The analysis shows that the first waves are relatively insensitive to the details of the earthquake fault plane parameters. Simulation results for unit sources have been stored as an online database with a WWW interface. A database user can quickly obtain a model prediction of the offshore tsunami wave heights at selected locations for a wide variety of AASZ earthquake scenarios. This database provides a useful offshore tsunami forecasting tool for hazard mitigation managers.

1. Background and Motivation

This study has been conducted as part of an effort to provide the Pacific Disaster Center (PDC) with tsunami forecasting capabilities. PDC is a joint Department of Defense and State of Hawaii activity, initially established in February 1996. The purpose of this center is to provide a source of information and guidance for all disaster-related events. It is currently in the process of acquiring tools to provide this capability for selected categories of disasters, including tsunamis [see URL http://www.pdc.org].

Potentially, the best approach to forecasting the impact of a particular tsunami event on a specific coastal site is to perform real-time tsunami model simulations that include real-time data assimilation. With such a capability, forecasts of tsunami impact would be computed immediately following a potentially tsunamigenic earthquake. As a community, we should work toward this difficult "Holy Grail" of tsunami forecasting. However, insufficient real-time earthquake data and a lack of confidence in tsunami generation and inundation modeling presently render the implementation of such an operational capability imprudent.

Fortunately, however, existing numerical models are good enough to provide useful guidance, if exercised with care by an experienced tsunami modeler. Event- and site-specific inundation estimates can be computed far in advance of the earthquake, thoroughly tested and scrutinized for reasonableness and sensitivity to errors, and then stored as a database. When an event occurs, the appropriate pre-computed results can be recalled, modified by data assimilation schemes that utilize a user-friendly interface to incorporate real-time tsunami measurements, and made available to aid hazard assessment and evacuation decision-making.

Such a database of pre-computed results cannot contain all possible tsunami events, simply because there is too much variability in the mechanism of tsunamigenic earthquakes. The database must contain a finite

number of events chosen from an infinite number of possible scenarios. A study of tsunami wave sensitivity to parameters of their earthquake sources can provide guidance for selecting events for the database. In particular, the sensitivity study can identify earthquake parameters that are not critical in determining the heights, periods and directionality of the resulting tsunamis.

Tsunami generation is commonly modeled by assuming that the initial sea surface displacement is formed by the permanent vertical displacement of the ocean bottom induced by an earthquake. The shape of the earthquake's vertical displacement can be inferred by applying a so-called "double-couple" source model and computing the elastic deformation of the earth's crust (e.g., Okada, 1985). This approach assumes that an earthquake can be modeled as the rupture of a single rectangular fault plane that is characterized by parameters describing the location, orientation, and rupture direction of the plane. These parameters are the length of the rupture plane L, the width of the plane W, the depth of the source h, dip angle δ, slip angle λ, strike angle θ, and the average slip amount u_0. The moment magnitude of this model source is determined by the formula

$$M_0 = \mu u_0 L W, \tag{1}$$

where μ is the rigidity of the earth crust with a value ranging from 1 to 6 $\times 10^{10}$ N/m^2, depending on the local geological structure (in this study, we use a value of 4.5×10^{10} N/m^2). The moment magnitude of the earthquake source, as well as its depth, dip angle, slip angle, and strike angle, are obtained from the moment tensor analysis of seismic waves. Then Equation (1), together with ancillary data such as aftershock patterns, can then be used to estimate the L, W, and u_0 of the earthquake.

The double-couple source is a very simplified model of an earthquake. But estimates of the five parameters of the double-couple model are available fast enough after the earthquake to be relevant for tsunami mitigation. More sophisticated models include multiple sub-faults with parameters that vary along the multi-fault structure. This fine structure of a fault can be obtained only after months of data analysis, provided that enough high-quality data (including tsunami data) exist for a particular event. More general, non-double couple models of earthquakes are also emerging (Julian *et al.*, 1998).

One approach for constructing a database of pre-computed inundation estimates is to vary each parameter of an earthquake source model, including the location, and then compute inundation values for each scenario. Even with the elimination of certain mechanisms and very sparse incrementation of the parameters, such a database can be enormous. In spite of these difficulties, this approach is being tested by Japanese scientists for a new tsunami warning system in Japan (Tatehata, 1997).

We have taken a different approach based on a two-step methodology. First, linearity of the generation/propagation dynamics is exploited to develop an offshore forecast database of "basis" scenarios that can quickly be arithmetically combined to relate earthquake parameters to the height, period, and direction of a tsunami wave off the coast. Second, these results are used as input to non-linear transfer functions that have been developed to relate the offshore wave characteristics to inundation (and/or current speeds)

at specific sites in harbors or at sites along the open coast. The advantage of the transfer function approach is its flexibility and compactness.

In principle, an infinite number of tsunami propagation scenarios can be constructed by linear combinations of a finite number of pre-computed "basis" scenarios. The linearity of this first stage also greatly simplifies data assimilation schemes for determining a tsunami source from deep-ocean gage recordings. A sensitivity study is an essential part of this concept, since it determines which earthquake parameters are the most important for tsunami generation. This is done by quantifying the influence of variations of earthquake parameters on the characteristics of the resulting tsunami waves.

In this study, the focus is on the sensitivity of deep-water tsunamis near Hawaii to the parameters of underwater earthquakes in the Alaska-Aleutian Subduction Zone (AASZ). This region is a major source of destructive tsunamis that strike Hawaii. The inundation patterns of these tsunamis in Hawaii will be determined by work proposed for FY 1999. The FY 1998 work reported here can be thought of as providing the necessary open boundary conditions for the planned FY 1999 tsunami inundation modeling of the Hawaiian region.

2. Methodology of This Study

Tsunami sensitivity was analyzed by studying numerical simulation results of different earthquake scenarios. The numerical analysis is focused on the first wave of each tsunami. Analytical studies of cross-ocean tsunami propagation (Section 3) indicates that bathymetric features affect the first wave only weakly. The following wave train, on the other hand, is complicated because it includes reflected and refracted waves. Thus, the leading wave carries the most information about a tsunami source. At many Hawaiian sites, the first waves of historic tsunamis are frequently the highest and therefore the most destructive.

The offshore sensitivity analysis exploits the assumed linearity of the tsunami propagation process, which implies that multiplication by a constant or addition of another solution will produce a valid tsunami propagation scenario. This linear assumption works very well for tsunami propagation in the open ocean. Nonlinear effects only become important as the tsunami approaches a coastline, at the depth less than 100–200 m, or during propagation over a very long continental shelf. Nonlinearity becomes dominant during tsunami inundation.

Analytical methods are first used to investigate wave-trapping and reflection processes in the earthquake source regions and during the wave propagation across the Pacific. Resulting theoretical estimates serve as a valuable guide in the design of the numerical experiments and help to constrain the range of parameters in the subsequent simulations.

3.   Analytical Studies of Cross-Ocean Tsunami Propagation

A set of analytic and one-dimensional models were developed to help interpret the results of the MOST model and to verify the use of the Sandwell/ Smith bathymetry in this model. These models were also used to investigate wave-trapping and reflection processes in the earthquake source regions. These simplified models show that geometric spreading is the main process affecting the amplitudes of the first waves of a tsunami to propagate from the AASZ to the deep ocean off Hawaii. Geometric spreading is augmented by the wave refraction that occurs as the tsunami waves propagate over progressive deeper water, from just south of the Aleutian Trench to the vicinity of Hawaii. Although the bottom topography in the North Pacific includes large seamount fields and numerous escarpments, estimates of wave scattering indicate that this fine-scale topography does not attenuate the first tsunami waves substantially. This is because these topographic features do not extend over a major fraction of the water column and their spatial scales are very short compared with a tsunami wavelength. The exception is the Emperor Seamount Chain/Hawaiian Ridge, which is seen in the MOST simulations. These features produce significant wave channeling. The deep-water scattering by very fine bathymetric features does not substantially attenuate the first tsunami waves. Hence, the spatial resolution and accuracy of the Sandwell/Smith bathymetry is fully adequate for use in the development of the tsunami database.

3.1   Analytic Theory

The analytic theory uses idealized tsunami waves incident on idealized bottom topography to better understand and scale tsunami wave reflection and scattering. The derivation of a formula for the reflected wave generated over lineal bathymetric features shows that its amplitude depends on the bottom slope, water depth, incident angle, and the horizontal scale of the features relative to the wavelength λ. For normal incidence on a submarine ridge with Gaussian cross-section, the maximum scattered energy is proportional to ϵ^2, the square of the height of ridge relative to the surrounding water depth. The maximum occurs approximately when $k\sigma = \sqrt{2}$, where $k = 2\pi/\lambda$ is the wavenumber off the ridge and σ is the half-width scale of the ridge. At longer tsunami wavelengths (lower frequencies) the amount of scattering decreases significantly with increasing wavelength. The application of this ridge theory is made later in this section for ridge-like features associated with the Mendocino Escarpment, the highest short-scale feature encountered by tsunamis propagating from the AASZ to Hawaii.

For circularly symmetric seamounts, the energy flux of the scattered wave is also proportional to ϵ^2. This type of scattering is weak in the open North Pacific between the AASZ and Hawaii since the seamounts here do not extend far up into the water column and they are very small compared with tsunami wavelengths. What scattering occurs is very sensitive ($\sim \omega^5$) to wave frequency ω, i.e., scattering effects are much stronger for

high-frequency waves. Since the seamounts in the North Pacific generally occur in irregular patterns, the amount of energy scattered from a tsunami propagating through a field of seamounts (e.g., the Alaska Seamounts) can be found by assuming that the scattering from one seamount is independent of the scattering from the others. This scattering, like that of the lineal ridges, is included in the MOST model simulation, since the Sandwell/Smith bathymetry in the model resolves these short-scale features.

3.2 One-Dimensional Monochromatic Model

The one-dimensional (1-D) numerical model solves the linear, inviscid shallow-water wave equations at a given wave frequency and alongshore wavenumber. The results are the surface elevation and water velocities as functions of the offshore (southward) distance from the AASZ. The numerical method adjusts the spatial increment so that the solutions are accurate within a preset limit δ. In the results described below, the equations are solved using double precision calculations, with δ set to 10^{-9}. For idealized bathymetry, the model is found to compute solutions that match analytic solutions to this accuracy.

Two types of coastal boundary conditions are used: a sloping beach to allow coastal reflection in the Alaska Peninsula region and an open-boundary condition to allow northward-propagating waves in the Aleutian Arc region to pass freely into the Bering Sea. The beach-condition provides information about coastal reflection and nearshore amplification, as well as bathymetric trapping near the earthquake source. The open-boundary condition allows a study of offshore wave reflection in the shelf/slope/trench region; it is also used to study wave scattering and refraction in the open North Pacific between the AASZ and Hawaii.

3.3 Model Testing Using Gulf of Alaska Tides

Since the tides are also shallow water waves and there are extensive tidal observations in the northern Gulf of Alaska that have been made by PMEL, it is appropriate to test the 1-D model against these observations. The observations were taken at 36 bottom pressure stations in a region ($51°$–$55°$N, $154°$–$159°$W) that extends from the lower continental slope, across the Aleutian Trench and onto the abyssal region. The 1-D model was solved along the $315°$T transect for largest diurnal (K1) and semidiurnal (M2) tidal constituents. It was tuned to the amplitude and phases of these tides at a single station, with the complex alongshore wavelength adjusted to match the alongshore distributions of these constituents. The Coriolis effect is included in the model because it strongly affects tides in the open ocean.

The results show close agreement between along-transect tidal distributions between the model and the observations. For an average over the 36 stations, the model values differed from the observations by only 0.1% and 0.3% in amplitude and $0.2°$ and $0.06°$ in phase for K1 and M2, respectively. The largest deviations occurred at the stations farthest from the transect (M2: 3.2%, $4.2°$), due to an assumption of pure wave propagation in the

alongshore direction. There is also close agreement of the tuned 1-D model tides with the latest global tidal models.

3.4   AASZ Source Region

The results of the 1-D tsunami simulations in the AASZ Source Region show that near-source wave trapping is significant only for waves propagating nearly alongshore. Because the AASZ fault zones are roughly parallel to this direction, the tsunami waves are primarily directed perpendicular to it (and toward Hawaii). Hence, this type of trapping does not substantially affect the first tsunami waves. There will be trapping and scattering of some waves, which will complicate the pattern of the later wavetrain and extend its duration in time. The Aleutian Trench has little effect on tsunami waves propagating directly across it, but does enhance wave trapping for the wave components propagating nearly parallel to the Trench.

For tsunamis generated on the continental slope, the northward-propagating component will be reflected only slightly (reflected wave amplitude $\sim$2–3% for a normally incident wave with a period of 20 minutes) on the upper slope/outer shelf region. Reflections of tsunami waves in the Aleutian Arc region are therefore due primarily to island reflections and resonance, rather than reflection at the shallow-to-deep-water transition between the Arc and the Bering Basin.

3.5   Deep North Pacific Between the AASZ and Hawaii

The amplitudes of tsunami waves propagating from the AASZ and the vicinity of Hawaii decrease primarily in response to cylindrical spreading from a source of limited spatial extent. This decrease amounts to $\sim$76%, with an additional 4% decrease due to refractive (Snell's Law) spreading. East-West escarpments and seamounts scatter only a small fraction of the energy of southward-propagating tsunami waves.

Computations based on the dispersion relation for gravity waves shows that differences in propagation times is negligible for wave periods greater than 10 minutes. This is for propagation in deep water from the Aleutian Trench to the Hawaii Rise. Longer period waves are expected for major tsunamigenic earthquakes in the AASZ. This result supports the assumption in the MOST model that non-dispersive wave theory applies to the major AASZ tsunami events.

The application of the ridge theory to ridge-like features associated with the Mendocino Escarpment (at 157°W) shows that the highest of these features has a maximum scattering energy of 2×10^{-4} relative to the incident energy. Hence, very little energy is scattered from the incident wave by these ridge features. The southward increase in water depth across the whole escarpment occurs over too large a distance at 157°W to scatter significant tsunami energy. However, near the U.S. West Coast, this distance becomes much shorter and the relative depth contrast across the Mendocino Escarpment becomes much larger. Hence, the Escarpment can be expected to interact significantly with tsunamis incident on the West Coast.

4. Numerical Study of Tsunami Sensitivity to Source Parameters

How sensitive are far-field tsunami model time series to changes in the source parameters? In the limit, the generation region will look more and more like a point source, so that the time series should become less and less sensitive to details of the source as the distance increases. This issue is central to the whole notion of a pre-computed forecasting database, since source parameters available only a short time after an earthquake occurs are preliminary in nature and may be somewhat inaccurate. To explore this question, an analysis was performed that exploited the availability of deep ocean tsunami time series collected in the far-field.

The MOST generation and propagation model has been tested against the deep-ocean data from bottom pressure recorders (BPRs) collected after the June 10, 1996 Andreanov Island tsunami; excellent agreement with observations was obtained (Titov and González, 1997). Since the Andreanov tsunami was generated in the AASZ, our area of interest here, and since this event is considered to be a typical subduction zone tsunamigenic earthquake (Tanioka and González, 1998), it was chosen as a "reference point" for this study. In particular, we wish to explore the sensitivity of the model simulations to changes in the earthquake parameters—i.e., how much could we change these parameters before the model-data comparison was unsatisfactory?

To reduce the number of parameters to a manageable level, certain reasonable assumptions were made about the fault plane models. First, the upper edge of each fault plane was set to the shallow depth of 5 km, since large subduction earthquakes with shallow faulting are believed to be the most effective in generating tsunamis. Second, we set the strike to align with the Aleutian Trench, since this appears to be true of most large underthrust earthquakes in the AASZ. As a third, important constraint, all model sources were required to have a fixed seismic moment M_0 equal to the estimated moment of the Andreanov earthquake of 7.3×10^{20} N m.

With these constraints, the sensitivity analysis is restricted to variations of the position of the earthquake epicenter along the AASZ and the four fault plane parameters *length, width, dip angle,* and *slip angle* that are varied about the reference *length* = 140 km, *width* = 70 km, *dip* = 20°, and *slip* = 108° used by Titov and González (1997). (Similar values of these parameters were estimated by Tanioka and González (1998) through comparison of the computed tsunami with near-source coastal tide gage data.) With these parameters set, the mean slip, u_0, is determined by means of the moment magnitude relationship, equation (1).

This study was conducted in two parts. First, model simulations were performed in which the Andreanov fault plane model of Titov and González (1997) was placed in different locations along the AASZ; this tested the sensitivity of the results to epicentral position. Second, model simulations were done for fault plane models located at the Andreanov earthquake epicenter, but with variations in the length, width, dip angle, and slip angle.
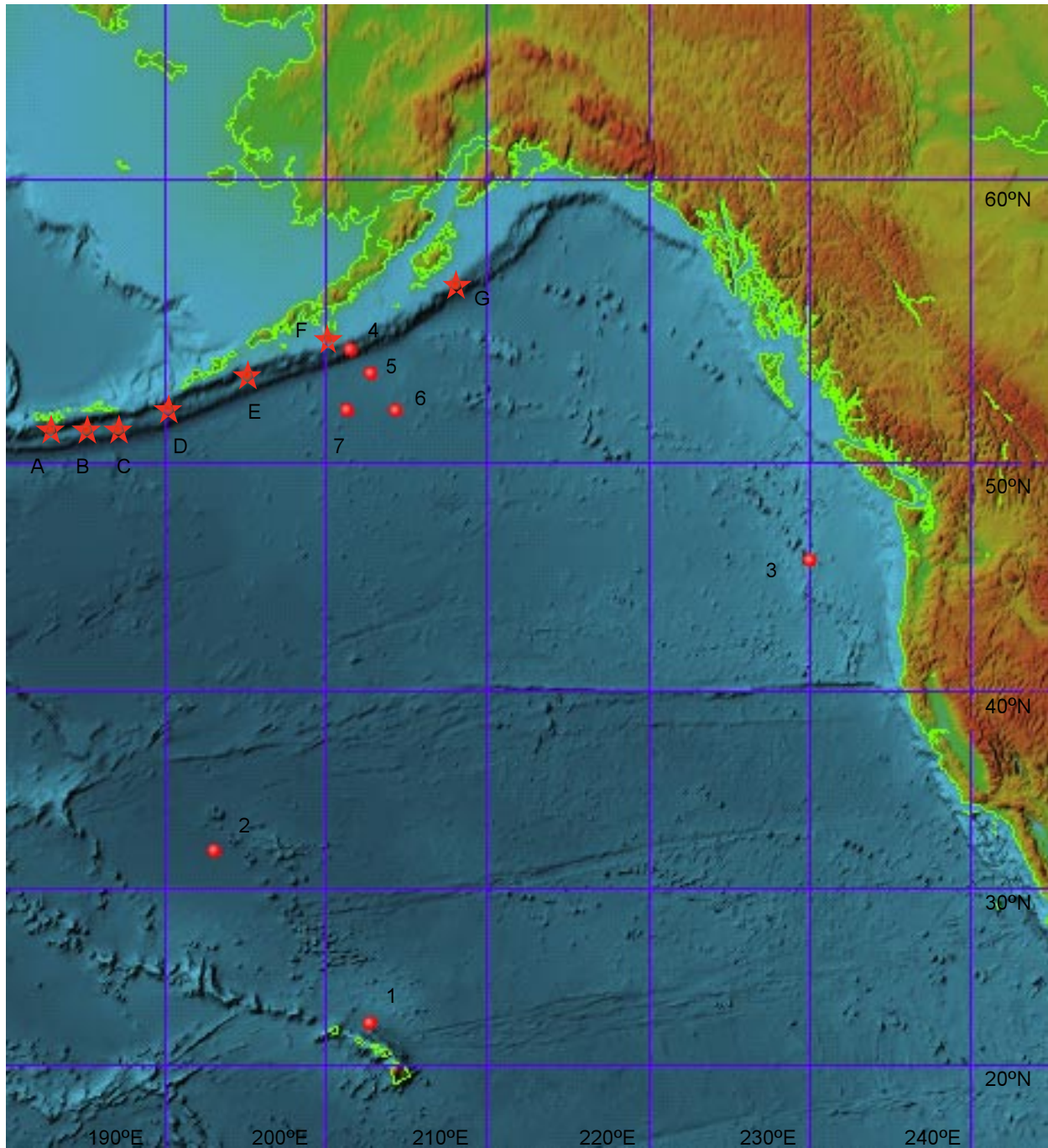
Figure 1: The locations of the earthquake sources and wave gages for the sensitivity study computations shown with the bathymetry of the computational area.

Table 1: Model source parameters for the study of tsunami sensitivity to earthquake location. The seismic moment magnitude is the same as that of the 1996 Andreanov earthquake for each case.

Sources	Long.	Lat.	Length	Width	Strike	Dip	Rake	Depth	Slip
A	51.2°N	182.7°E	140 km	70 km	260°	20°	108°	5 km	2 m
B	51.2°N	185.0°E	140 km	70 km	253°	20°	108°	5 km	2 m
C	51.2°N	187.0°E	140 km	70 km	253°	20°	108°	5 km	2 m
D	52.0°N	190.0°E	140 km	70 km	253°	20°	108°	5 km	2 m
E	53.3°N	195.0°E	140 km	70 km	245°	20°	108°	5 km	2 m
F	54.1°N	200.0°E	140 km	70 km	238°	20°	108°	5 km	2 m
G	56.5°N	208.0°E	140 km	70 km	230°	20°	108°	5 km	2 m

Computed tsunami time series were saved at the locations shown in Figure 1, and our analysis concentrated on Gage 1 near Hawaii, Gage 2 between Hawaii and the AASZ, and Gage 3 off the West Coast. Both locations are in deep water where the wave dynamics are linear; Gage 1 is at 4747 m depth and Gage 2 is at 5910 m. Other important locations shown in Figure 1 are positions of the bottom pressure recorders (BPR) where the time series of the Andreanov tsunami were recorded and compared with the MOST simulations. Gage 3 is located on Axial Seamount, at a depth of 1550 m.

4.1 Sensitivity to Earthquake Location

The position of the earthquake epicenter is one of the most important parameters in determining the characteristics of the resulting tsunamis. A series of numerical experiments were performed to quantify the effect of the earthquake positioning on the tsunami characteristics near Hawaii and off the West Coast. Seven different earthquake locations were modeled. The strike direction for each source is adjusted to align the sources along the Aleutian Trench. Positions of the sources are shown on Figure 1, and the fault plane parameters are summarized in Table 1.

Figure 2 shows results of numerical simulations for the sources listed in Table 1. For the purpose of comparison, the time scale of all computed tsunamis, except for the Andreanov record, has been moved to the same arrival time. Time series at Gages 2 and 3 show that the first wave amplitude varies significantly with source location. At Gage 2, the amplitude of the first wave decreases gradually when the source location is moved eastward. For instance, the tsunami generated by the western-most source A has 2.7 times higher amplitude than the wave from the eastern-most source G. At Gage 3, the effect is inverted and amplified: the largest wave generated by the source G has 5.5 times higher amplitude than the smallest wave generated at source A.

One obvious reason for the decrease of amplitudes is cylindrical spreading, which causes tsunami wave amplitudes to decrease with distance from the source. Another reason is the directionality of the tsunami wave pattern. The shape of a tsunami source and the bathymetric profile near subduction zones make tsunami energy very directional, with most of the wave energy
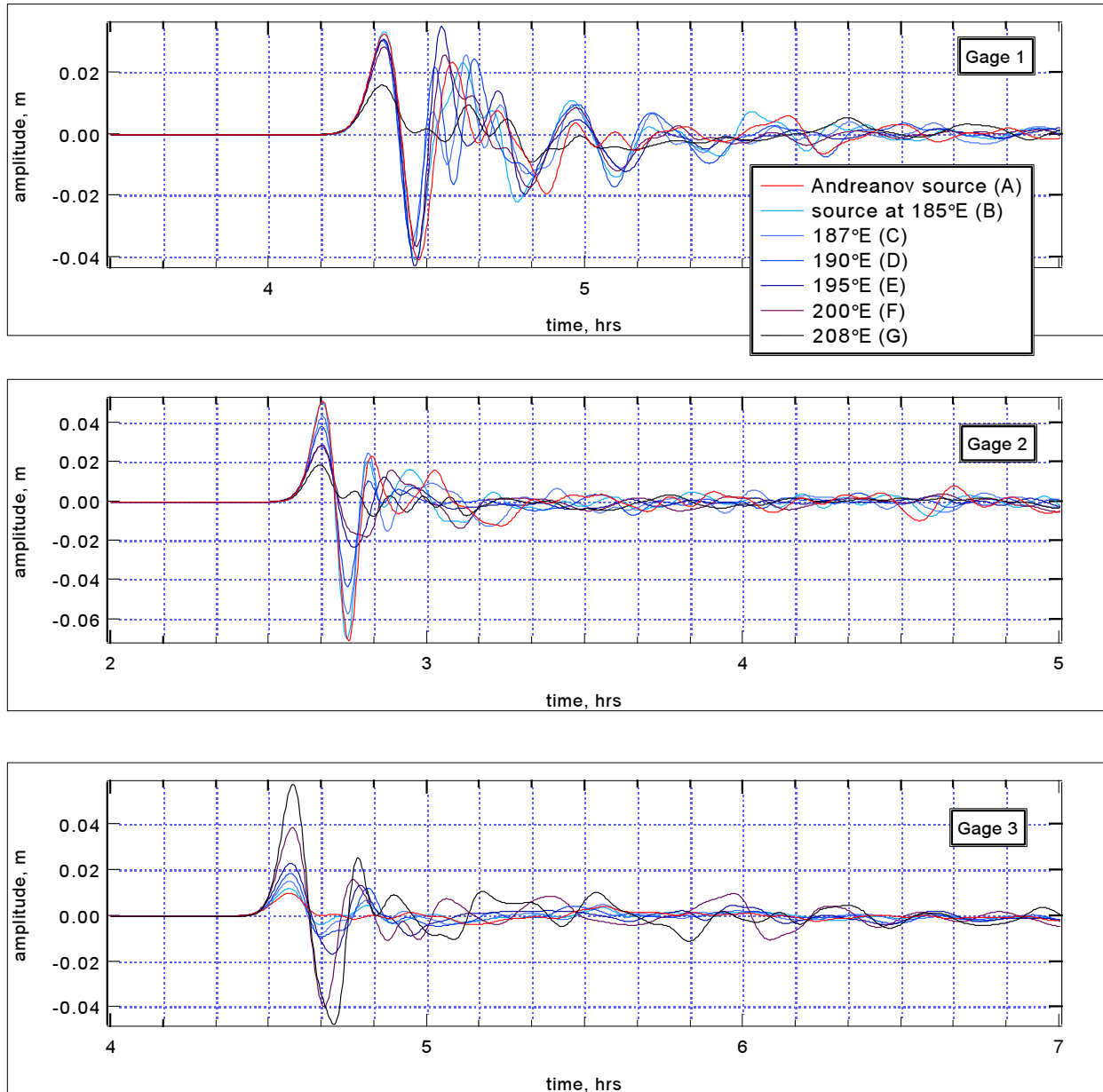
Figure 2: Tsunami time series at gages 1, 2, and 3 computed for different source locations. The time scale of all computed tsunamis, except for the Andreanov record, has been moved to the same arrival time.

Table 2: Model source parameters for the study of tsunami sensitivity to fault dimensions. The locations of the epicenters are the same as that of the 1996 Andreanov earthquake.

Sources	Long.	Lat.	Length	Width	Strike	Dip	Rake	Depth	Slip
H	51.2°N	182.7°E	140 km	70 km	260°	20°	108°	5 km	2 m
I	51.2°N	182.7°E	140 km	105 km	260°	20°	108°	5 km	1.3 m
G	51.2°N	182.7°E	200 km	70 km	260°	20°	108°	5 km	1.4 m
K	51.2°N	182.7°E	105 km	70 km	260°	20°	108°	5 km	2.7 m
L	51.2°N	182.7°E	140 km	35 km	260°	20°	108°	5 km	4 m
M	51.2°N	182.7°E	70 km	70 km	260°	20°	108°	5 km	4 m

propagating at right angles to the earthquake fault. This effect is demonstrated in Figure 3, where contours of maximum computed amplitudes are presented for two sources A and G. The amplitude of the off-shore propagating tsunami is larger in the direction perpendicular to the trench (and the tsunamigenic fault). The farther away the site is from this main beam, the smaller the amplitudes of the waves are, even if the site is fairly close to the source.

Amplitudes of the first waves at Gage 1, the nearest to Hawaii, are very similar for almost all the sources. The only exception is source G, which generated half the tsunami amplitude at Gage 3 as compared with the other sources. The bathymetry of the area around source G is quite different from the other source locations. There are a series of seamounts in the Gulf of Alaska that can affect the propagation from that source. Also, some of the tsunami energy generated by source G appeared to be trapped by the shallow bathymetry off the West Coast.

The period and the shape of the leading tsunami waves for different sources are quite similar at all the gages. In contrast, the wave train following the first wave is quite unique for each source. This wave train is formed by interference patterns of tsunami waves that have taken different propagation paths to the gage. Reflections from bathymetric features that determine the appearance of the wave train appear to have little influence on the leading wave, confirming the analytical results described in Section 3.

4.2 Sensitivity to Fault Dimensions

The dimensions of a fault plane can only be estimated with reasonable accuracy when indirect data, such as a three-dimensional aftershock distribution, is available and analyzed. It takes months, or even years, after the earthquake to obtain such information. The problem of rapidly estimating rupture-size is still unresolved. Presently, the only means of quickly estimating fault size for a real-time tsunami assessment are several empirical formulas that roughly evaluate the size and extent of rupture as a function of earthquake magnitude.

To determine the tsunami sensitivity to the dimensions of the fault plane, six different sets of dimensions were used. The slip amount of each has been adjusted to preserve the magnitude of the earthquake. Parameters of the
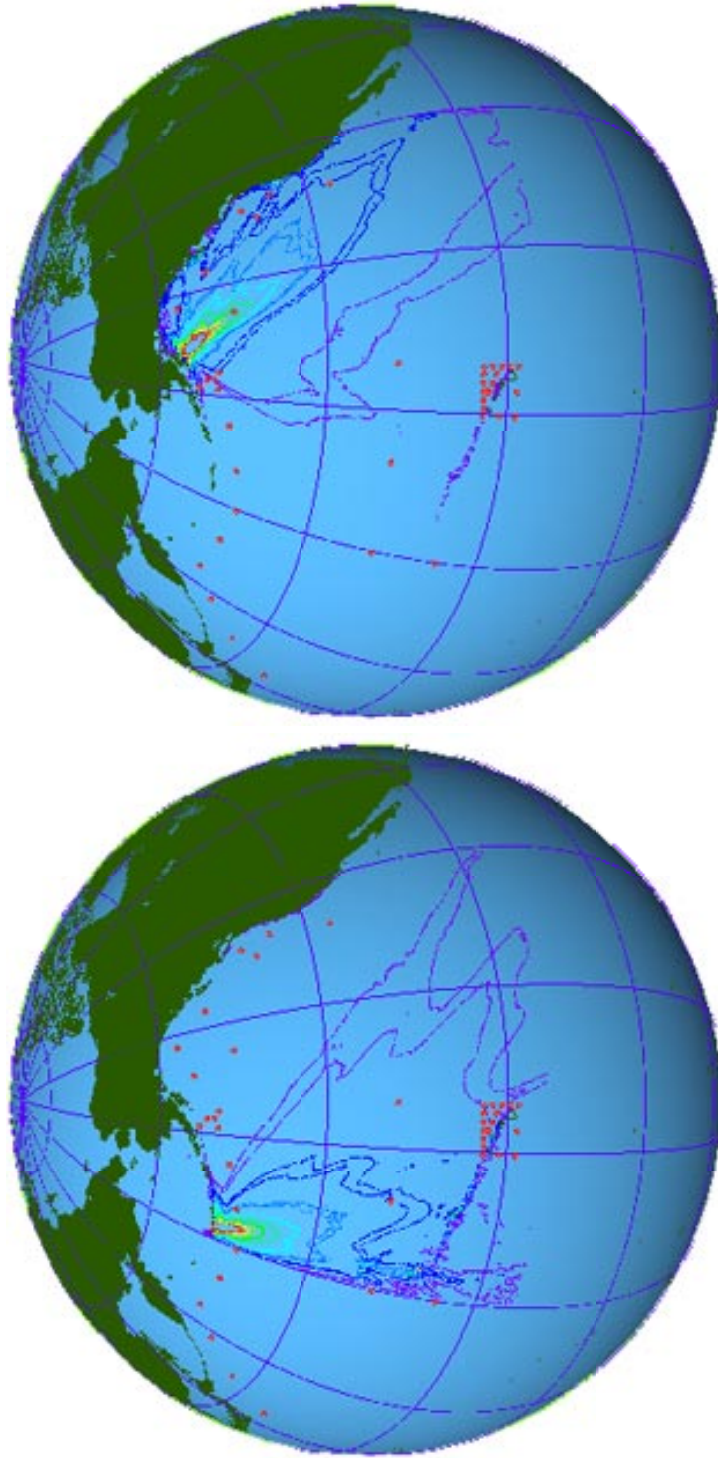
Figure 3: Contours of maximum computed tsunami amplitudes for source A (a) and source G (b). Contour intervals are 2 cm.

Table 3: Model source parameters for the study of tsunami sensitivity to dip and rake. The locations of the epicenters are the same as that of the 1996 Andreanov earthquake.

Sources	Long.	Lat.	Length	Width	Strike	Dip	Rake	Depth	Slip
N	$51.2°$N	$182.7°$E	140 km	70 km	$260°$	$20°$	$108°$	5 km	2 m
O	$51.2°$N	$182.7°$E	140 km	70 km	$260°$	$15°$	$108°$	5 km	2 m
P	$51.2°$N	$182.7°$E	140 km	70 km	$260°$	$10°$	$108°$	5 km	2 m
Q	$51.2°$N	$182.7°$E	140 km	70 km	$260°$	$20°$	$90°$	5 km	2 m
R	$51.2°$N	$182.7°$E	140 km	70 km	$260°$	$20°$	$100°$	5 km	2 m
S	$51.2°$N	$182.7°$E	140 km	70 km	$260°$	$20°$	$120°$	5 km	2 m
T	$51.2°$N	$182.7°$E	140 km	70 km	$260°$	$20°$	$135°$	5 km	2 m

model sources are summarized in Table 2. As seen in Figure 4, the leading waves at Gage 1 (near Hawaii) and Gage 2 (between Hawaii and Alaska) show very little sensitivity to the dimensions of the rupture plane. The difference in amplitudes of the leading waves is within 25% of the maximum, although the corresponding vertical displacements of the ocean bottom (and areas of the fault planes) differ by a factor of three. The variation between different solutions is larger at Gages 3 and 4, located near the continental coast. However, the leading waves from the different sources (Table 2) are within 50% of the maximum at these gages.

4.3   Sensitivity to Rake and Dip Angles

Several numerical experiments were conducted to study the influence (Table 3) of small variations in dip and rake angles on the tsunami waves, using the Andreanov source location. Figure 5 shows that lowering the dip angle from $20°$ to $10°$ (the typical range for subduction earthquakes in AASZ) leads to a 30% decrease in the amplitudes of leading tsunami waves. However, the period and the shape of the first wave stays very much the same for all dip angles.

   Variations in the rake angle do not affect the tsunami waves significantly (Figure 6). Five different rake angles are computed ranging from pure dip-slip mechanism (rake = $90°$) to a 50% strike-slip component in the fault motion (rake = $135°$). The smallest amplitude (rake = $135°$) is only 20% less than the largest (for rake = $90°$).

5.   Application to Tsunami Database Construction

The main purpose of the sensitivity study of the previous section was to provide guidance for the construction of a database consisting of pre-computed tsunami scenarios. The results demonstrate that, for a fixed location and magnitude, there is very weak dependence of the offshore tsunami characteristics on a reasonable range of other AASZ earthquake parameters. In all computed scenarios, the first wave amplitude does not differ from the observed Andreanov tsunami amplitude by more than 25%. The half-periods
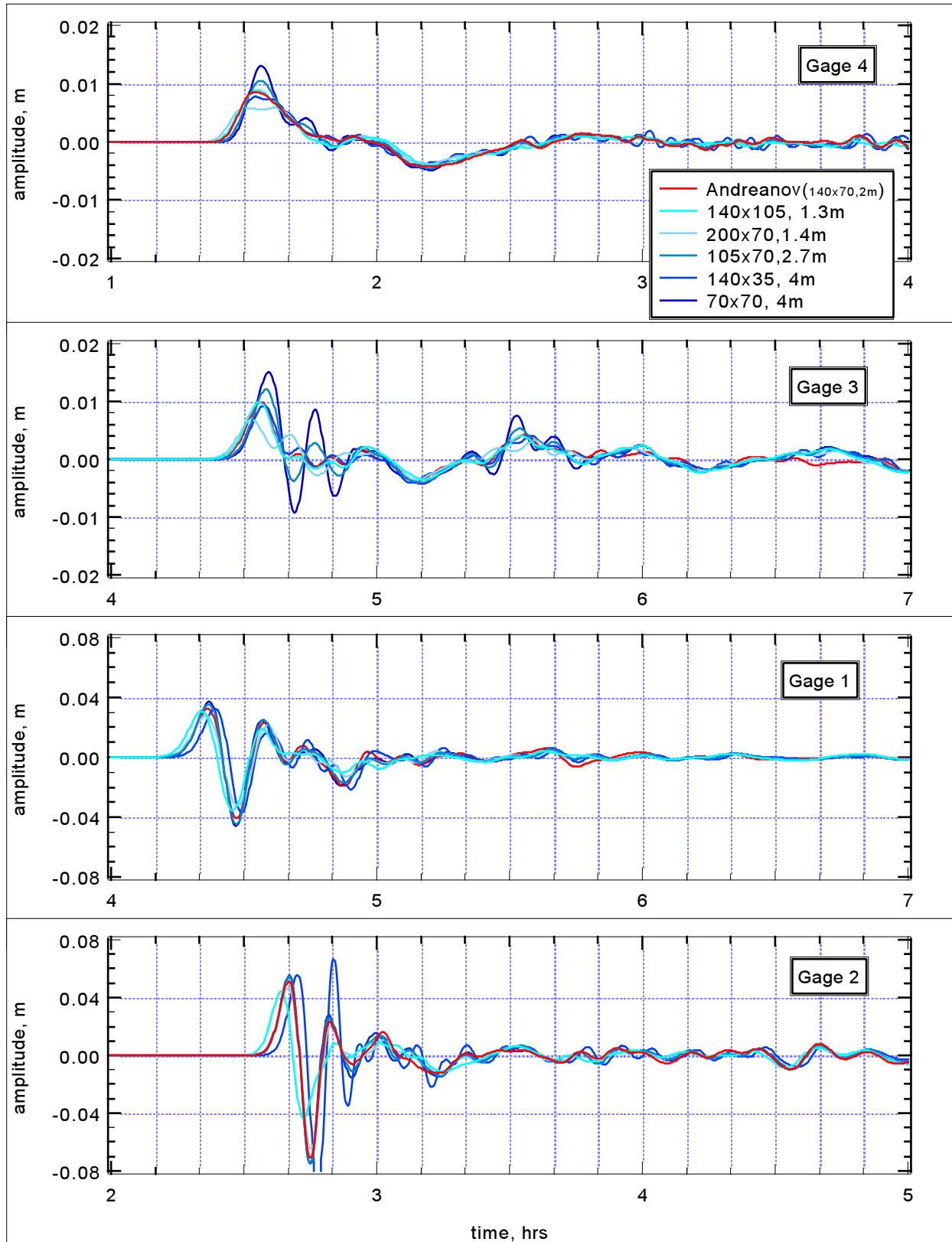
Figure 4: Tsunami time series at Gages 1, 2, 3, and 4 computed for different source dimensions. The slip amount of each source is adjusted to preserve the magnitude of the earthquake ($M_o = 7.3 \times 10^{20}$ N m).
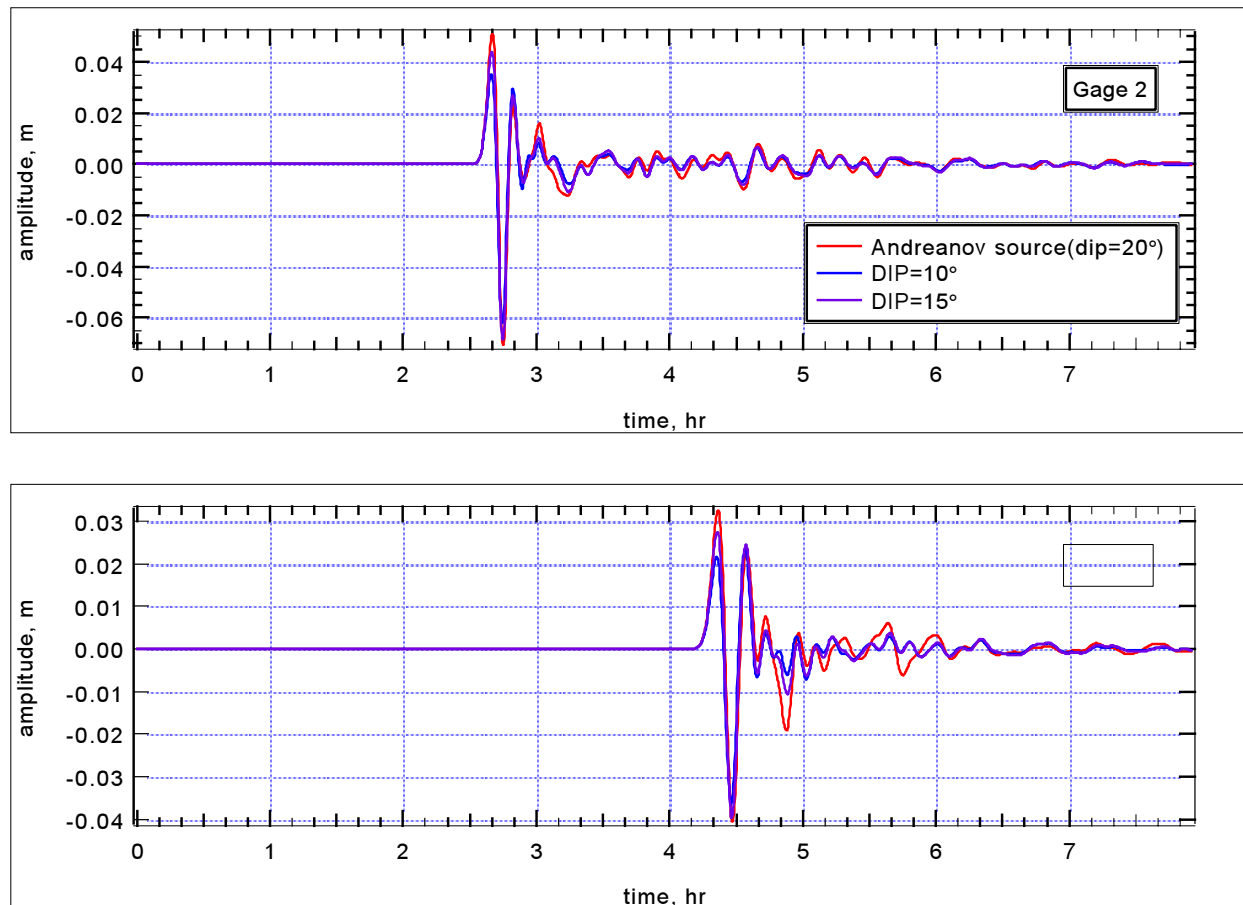
Figure 5: Tsunami time series at Gages 1 and 2 computed for different dip angles of the tsunami source.

are also within 5% of that of the Andreanov tsunami, and the shapes of the first waves are similar for all the sources. Hence, the leading tsunami waves generated by AASZ earthquakes are characterized in the far field mainly by the earthquake magnitude and location.

5.1   Method of Database Construction

A typical subduction mechanism for an $M_w = 7.5$ earthquake was chosen as the "unit source" for the model database. The parameters of the unit source are length = 100 km, width = 50 km, dip = 15°, rake = 90°, depth = 5 km, slip = 1 m. The strike of each source is adjusted to align the source along the local orientation of the subduction zone. The fault dimensions of 100×50 km^2 were chosen because they coincide with the size of observed AASZ asperities, which have been estimated to be the areas of actual vertical ground deformation associated with AASZ earthquakes (see review by Johnson, 1998). These unit sources are placed at locations along the AASZ 100 km apart from each other, forming a continuous line of faults along the Aleutian Trench (B-sources on Figure 7). A second line of similar sources (line A on Figure 7) is placed immediately north of the B-sources. To form a continuous fault plane, the epicenters of the A-sources are placed
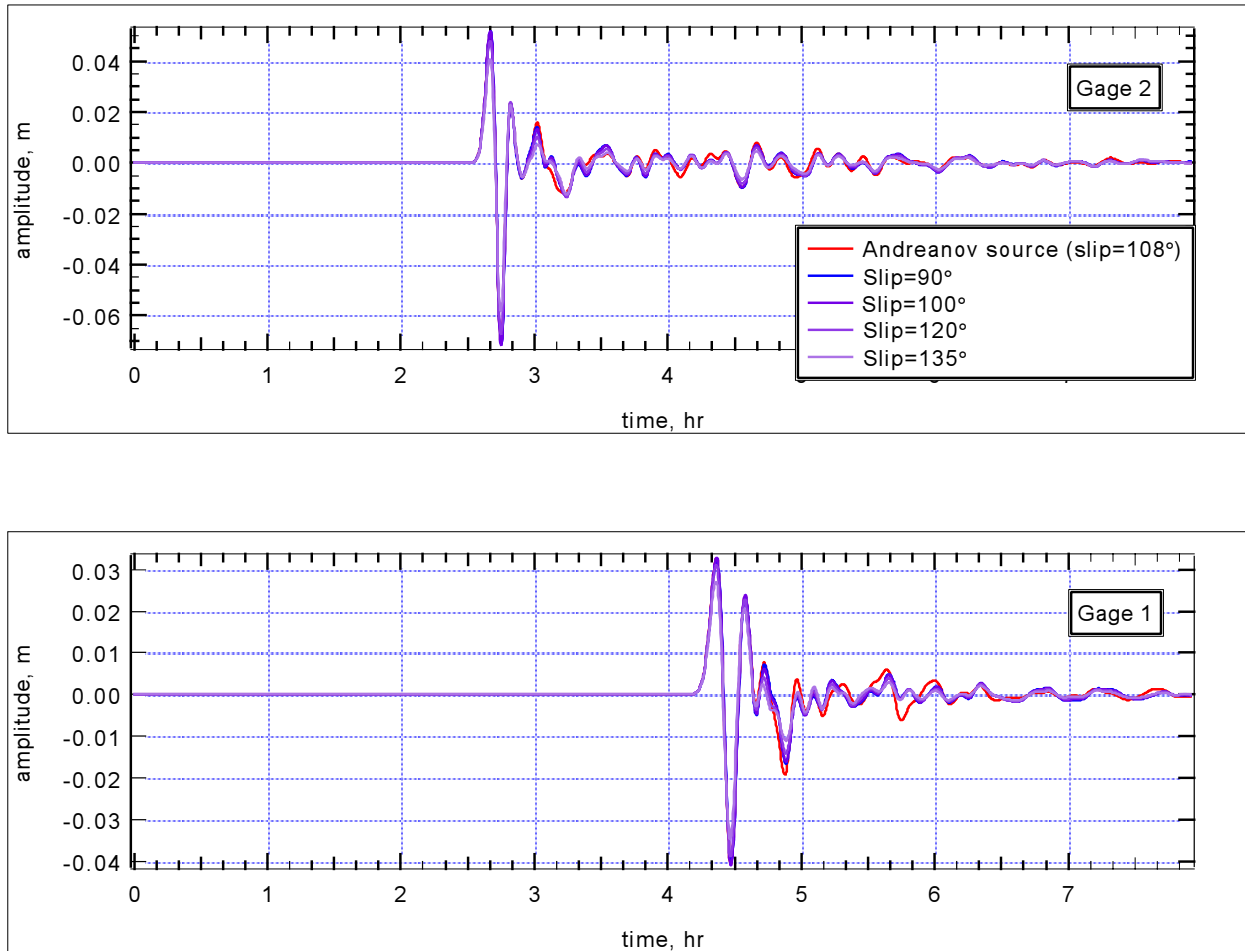
Figure 6: Tsunami time series at gages 1 and 2 computed for different rake angles of the tsunami source.

at a depth of 17.5 km (the depth of the north edge of B-faults). Tsunami propagation has been modeled for each unit source and the results of each simulation have been stored in the database. Computations were performed on a 4-minute bathymetric grid using a time step of 15 seconds. To reduce the database size and access time, the solutions are stored with a coarser sampling of 1° in space and 1 minute in time.

5.2   User Interface and Real-Time Data Assimilation

It is expected that real-time reports of tsunami wave heights will soon be available operationally in the open North Pacific during tsunami events (Milburn *et al.*, 1996). These direct tsunami observations can be combined with the forecast database to improve the accuracy of the tsunami forecast methodology. A flexible user interface has been developed that employs World Wide Web technology (`http://corona.pmel.noaa.gov/~tsunami/ model/`) and is designed with real-time data assimilation in mind. The interface exploits the linearity inherent in the tsunami forecast database. It greatly simplifies and speeds the addition of unit sources that are mul-
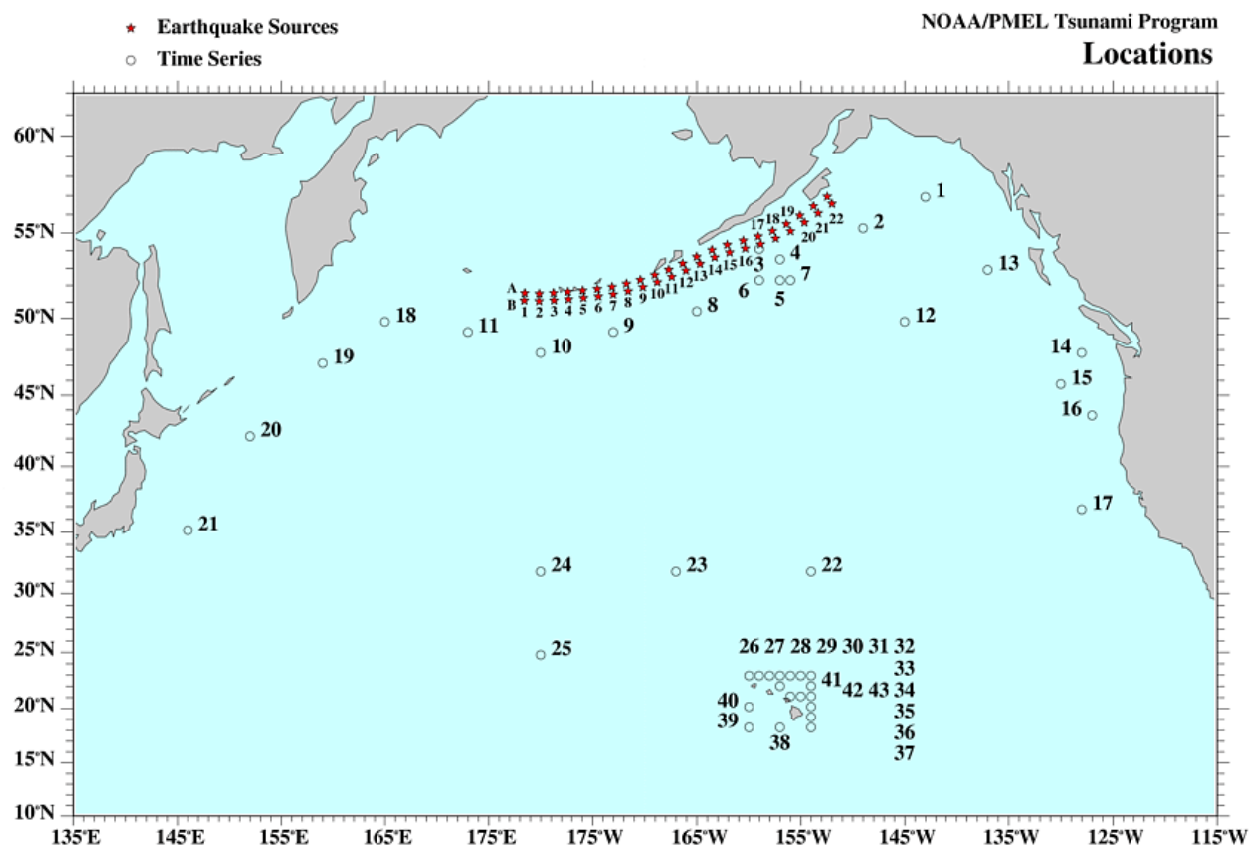
Figure 7: The locations of the unit tsunami sources along AASZ (stars) and preselected gage sites (open circles). Model results of tsunami propagation from these sources form the model database.

tiplied by factors to form larger fault planes characterizing a major earthquake. The multiplier for each unit solution can be different, thus simulating non-uniform slip distribution within the larger earthquake fault plane. The computed tsunami waveforms (Figure 8) are then quickly available for geographical coordinates corresponding to the locations of existing or planned real-time observations (as well as other locations near Hawaii and around the Pacific Rim). When the user (forecaster or emergency manager) obtains a satisfactory correspondence between computed and observed tsunami time series, a map of maximum computed amplitudes in the North Pacific can be examined to guide the forecast (Figure 9).

6. Future Plans

Prediction of tsunami inundation is the next logical step in the development of tsunami forecasting tools. Development of these inundation prediction tool is planned for FY 1999–2000 as a continuation of the current project. Site-specific sensitivity studies of inundation as a function of offshore tsunami characteristics will be performed, and an inundation database will be developed. The final goal is to integrate the results of this offshore tsunami sensi-
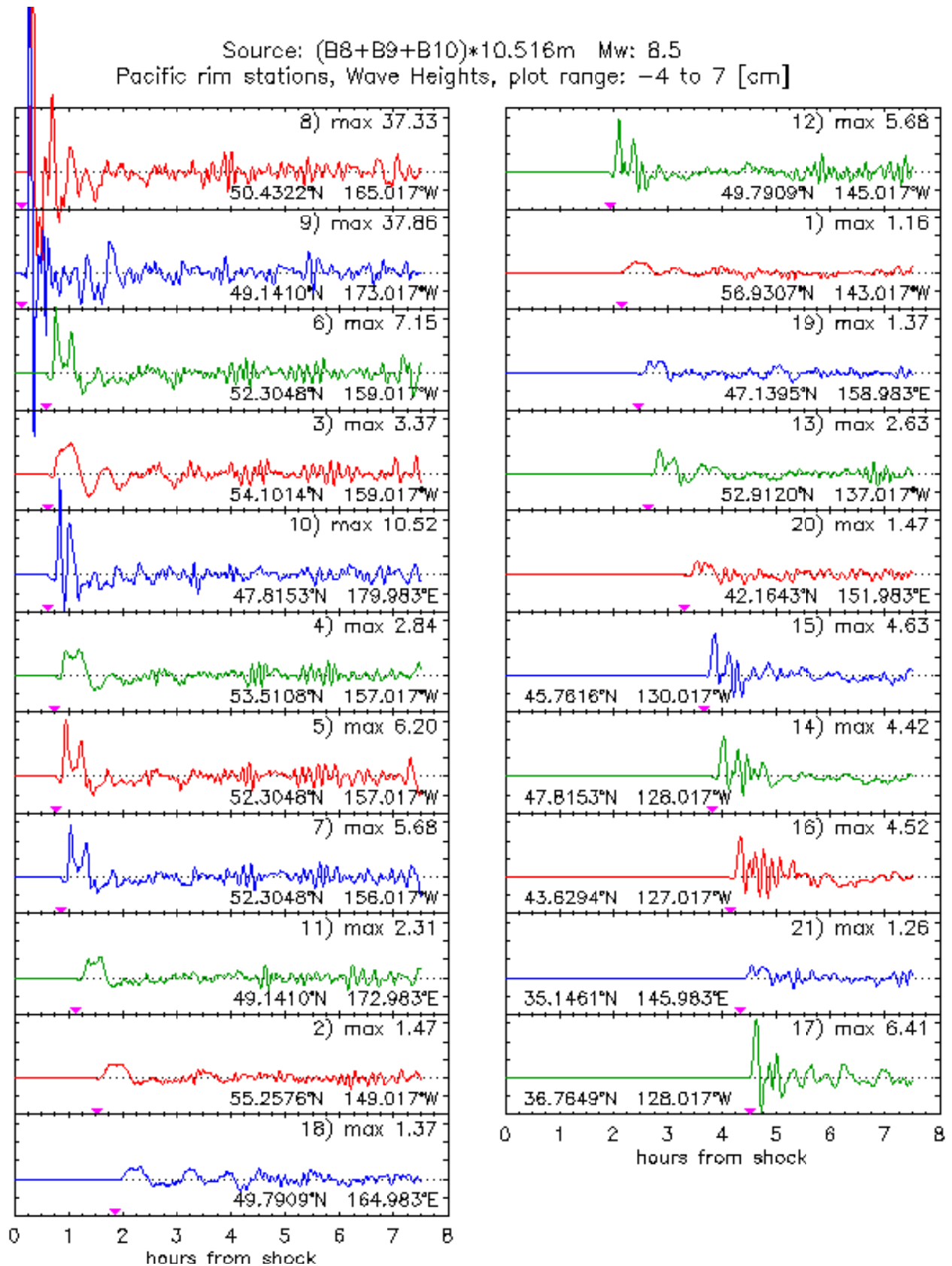
Figure 8: The waveform output of the tsunami model database. The waveforms are computed for the same tsunami source as in Figure 9, at the locations shown in Figure 7.
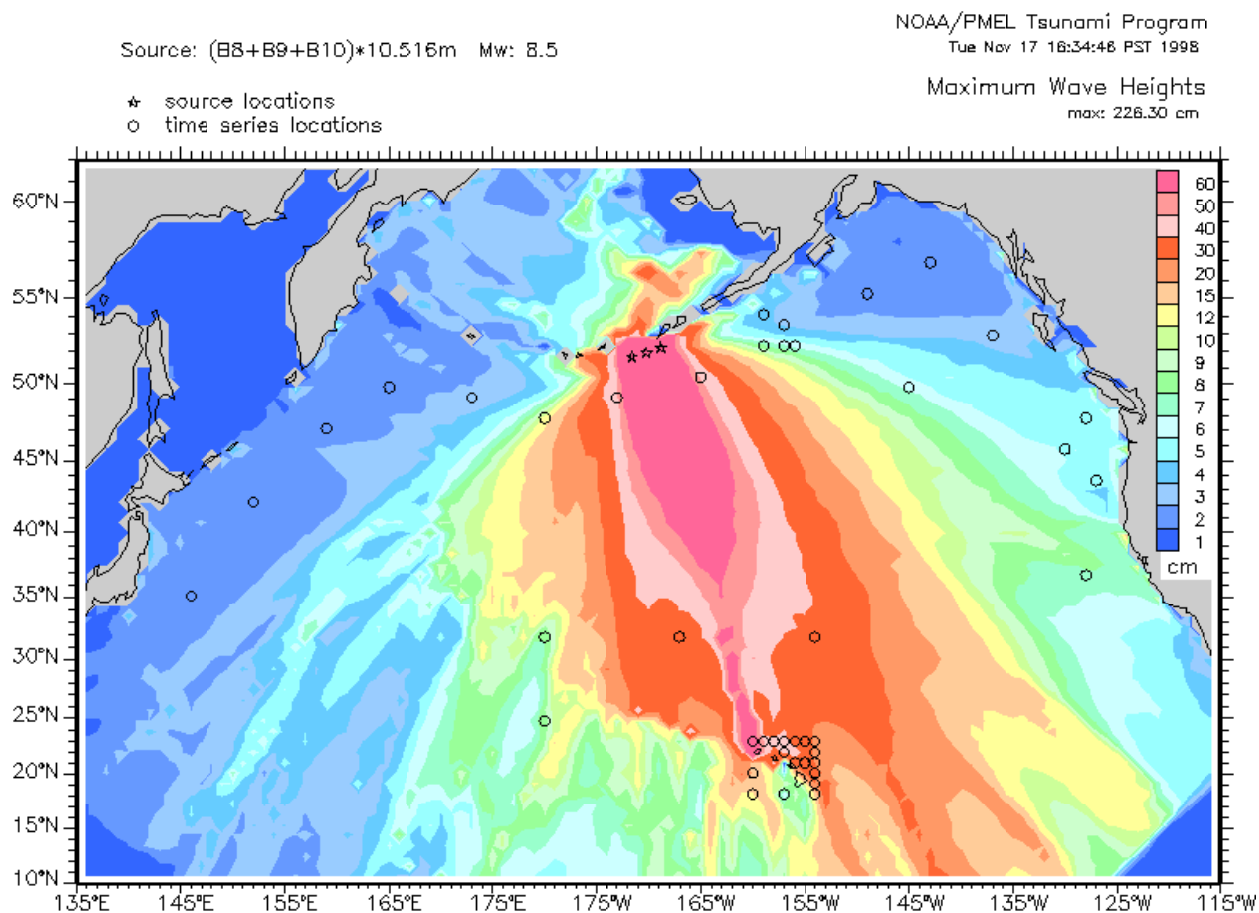
Figure 9: An example of the database output shows maximum computed wave heights produced by a tsunami in the computational area. The source of the tsunami is a combination of three unit sources (stars).

tivity study and the offshore forecast database with the inundation database and a real-time data assimilation scheme to produce a systematic methodology for tsunami forecasting guidance that is both source- and site-specific.

This work could also be extended to include pre-computed scenarios for sources along the entire Pacific Rim. For instance, the Kuril-Kamchatka and Japan Subduction Zones are very active and produce very strong tsunami-generating earthquakes almost every year. The Cascadia Subduction Zone is also active and capable of a mega-thrust event that would generate a large tsunami (e.g., Atwater, 1987). To add these potential sources to the database, a sensitivity study should be performed for each of the areas using the same methodology as for the AASZ sources. Then pre-computed scenarios could be used to forecast offshore tsunamis not only for the Hawaiian Islands but for all Pacific Rim coastlines included in the computations.

7. Acknowledgments

puter Center provided computer time and support for parallelization of the tsunami propagation model.

8.   References

Atwater, B.F. (1987): Evidence for great Holocene earthquakes along the outer coast of Washington State. *Science, 236,* 942–944.

Johnson, J. (1998): Heterogeneous coupling along the Alaska-Aleutians as inferred from tsunami, seismic, and geodetic inversions. *Advances in Geophysics, 39* (R. Dmowska, ed.), Academic Press.

Julian, B.R., A.D. Miller, and G.R. Foulger (1998): Non-double-couple earthquakes. *Rev. Geophys., 36*(4), 525–568.

Milburn, H.B., A.I. Nakamura, and F.I. González (1996): Real-time tsunami reporting from the deep ocean. Proceedings of the Oceans 96 MTS/IEEE Conference, 23–26 September 1996, Fort Lauderdale, FL, 390–394.

Okada, Y., 1985, Surface deformation due to shear and tensile faults in a half-space. *Bull. Seismol. Soc. Am., 75,* 1135–1154.

Tanioka, Y., and F.I. González (1997): The Aleutian earthquake of June 10, 1996 (Mw 7.9) ruptured parts of both the Andreanov and Delarof segments. *Geophys. Res. Lett., 25*(12), 2245–2248.

Tatehata, H. (1997): The new tsunami warning system of the Japan Meteorological Agency. In *Perspectives on Tsunami Hazard Reduction,* G. Hebenstreit (ed.), Kluwer, 175–188.

Titov, V.V., and F.I. González (1997): Implementation and testing of the Method of Splitting Tsunami (MOST) numerical model. NOAA Tech. Memo ERL PMEL-112 (PB98-122773), PMEL, Seattle, WA, 11 pp.

Appendix A: Notes on parallelization of the MOST propagation model

W. Smith and V.V. Titov

The propagation part of the MOST numerical model has been adapted for computations on a parallel supercomputer. The MOST code has been modified using Message Passing Interface (MPI) to perform parallel computations on distributed-memory machines. An IBM SP2 system at the Maui High Performance Computer Center (MHPCC) was used to perform the computations using the MOST parallel code.

A Master-Worker parallelization scheme has been adopted for the MOST parallel code. It appeared to be the least disruptive of the original code. The master passes a column to a worker node, then another column to another worker and so on until all the workers have a column to process (Figure A1). Then the master gathers the columns back up. This is repeated until no more columns exists. The process is repeated with the rows. The master doesn't do any of the computation, only the workers do.
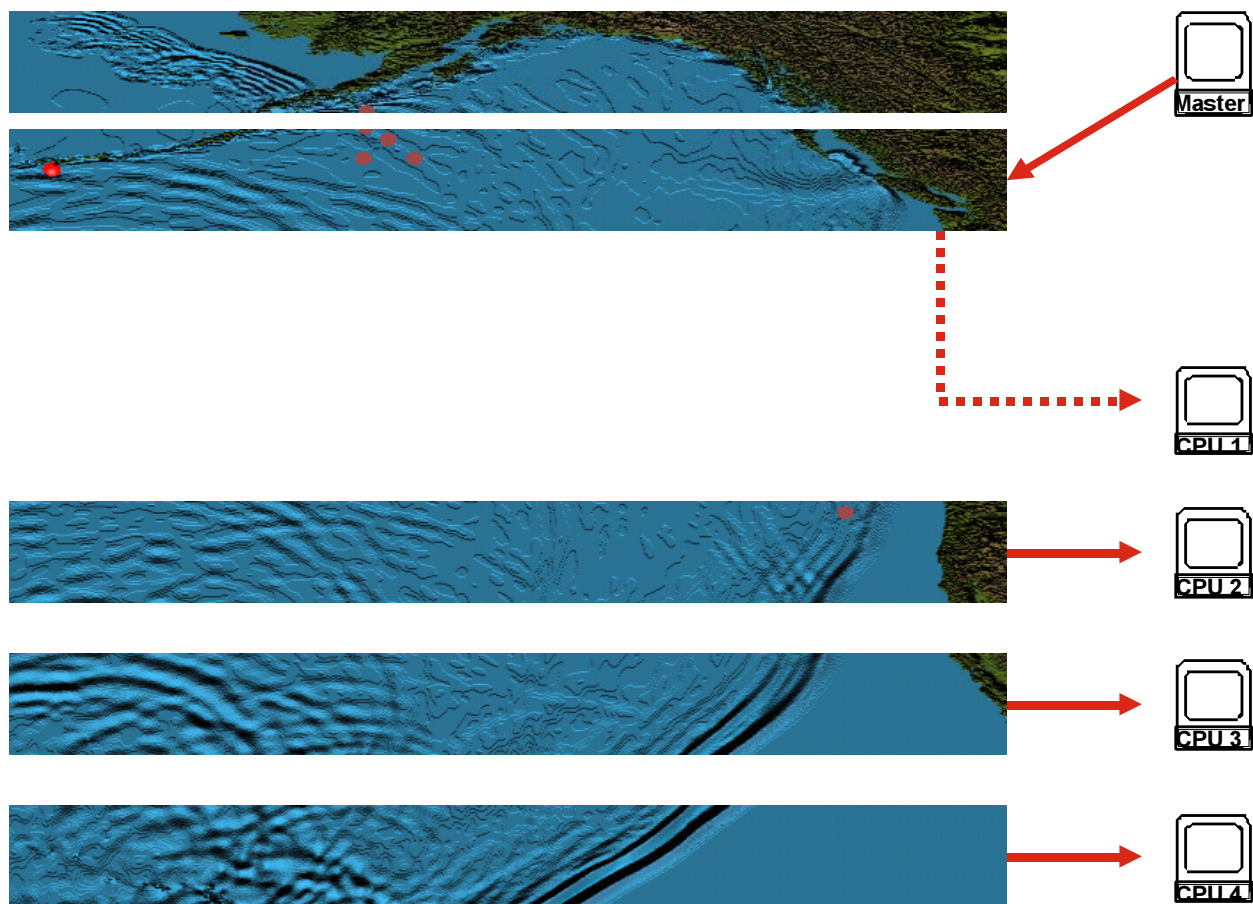

Figure A1: Master-Worker parallelization scheme applied for the MOST propagation code.
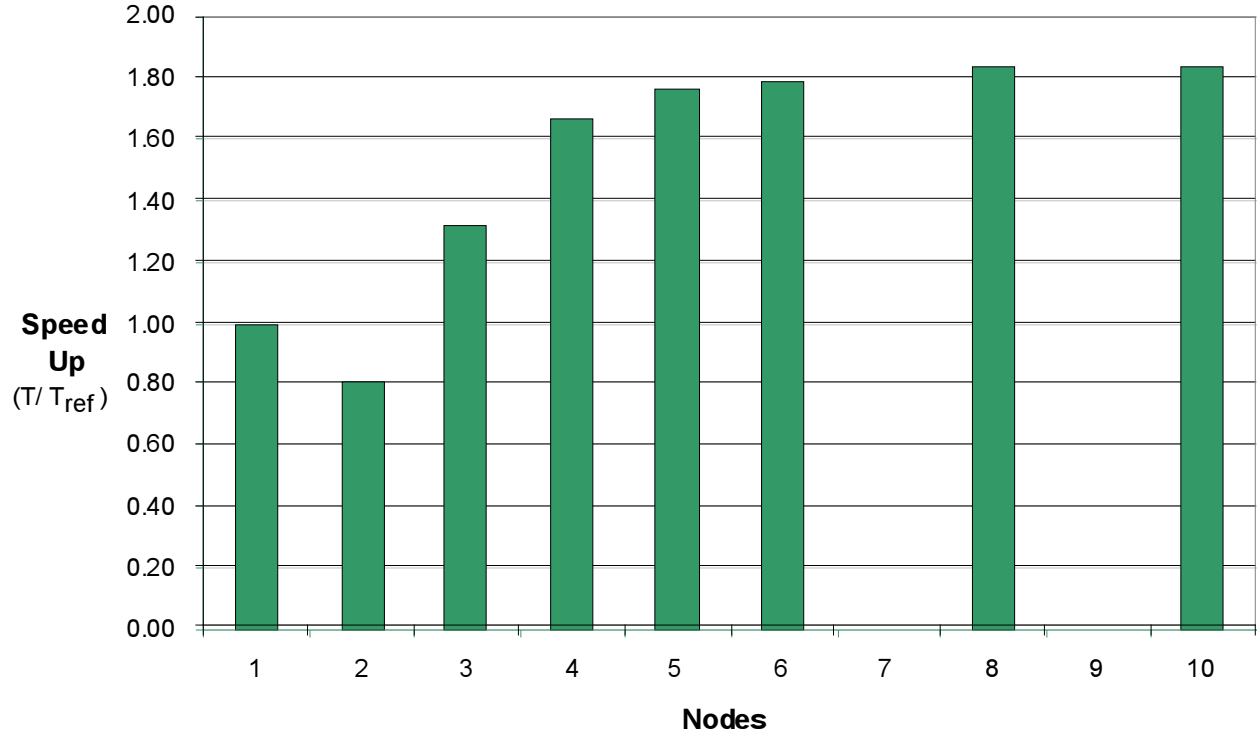
Figure A2: Speed-up of the MOST parallel code computed with different numbers of computer nodes.

In a test simulation, the non-parallelized code ran $T_{ref} = 1$ hour 28 minutes for 1000 time steps, which models 2 hours 45 minutes of tsunami propagation time. The parallelized code has been tested for different numbers of processors. Figure A2 shows the increase in speed obtained on the IBM SP2 parallel computer. The 5-node parallelized code ran in 50 minutes. It was a bit less than a 2X speed-up. It is expected that on larger data sets, the speed-up will be much greater. The master-worker parallelization is only the first attempt to adapt the MOST code for the parallel ccomputation. There are other methods of parallelization that can produce a much faster version of the code, such as non-blocking sends and receives, domain decomposition, and many others.

Future plans include further optimization of the MOST parallel code using domain decomposition method to obtain fast working propagation and inundation models. Application of nested grids during the inundation computation can produce a very efficient parallel algorithm, where all the sub-grids are computed simultaneously on different nodes. The data assimilation algorithm is another task where the full potential of the parallel computing can be exploited. It requires computing many independent tsunami scenarios at the same time in order to obtain an approximation of the tsunami source. These types of algorithms are usually very well suited for parallel computations.